Stratospheric polar cap-mean height and temperature as extended-range weather predictors

Peter Siegmund*

1 February 2005

*Corresponding author

Royal Netherlands Meteorological Institute

P.O. Box 201

3730 AE De Billt

The Netherlands

Email: siegmund@knmi.nl

Abstract

The skill of stratospheric and tropospheric predictors in predicting near-surface quantities at the extended range (~10 days-2 months) has been investigated, using 40 years of reanalysis data from the European Centre for Medium-Range Weather Forecasts. The predictors are 1) the geopotential height (Z) at various levels, 2) the difference between Z and the 1000 hPa-geopotential (Z-Z(1000)), and 3) the temperature at various levels. The predictors are averages over the area north of 65ºN. The predictands are Z(1000) averaged over the same area, and geographical fields of several near-surface quantities. The predictive skill has been investigated for different lead-times between predictor and predictand, and different averaging periods of the predictor and the predictand.

The results show that the predictive skill of Z in the troposphere is mainly due to the predictive skill of sea-level pressure, whereas the predictive skill of Z in the stratosphere is mainly due to the predictive skill of stratospheric temperature. The predictive skill is largest in the end of December, for the predictor Z at 50 hPa and the temperature between 250 and 50 hPa. The temperature has also significant predictive skill in the upper stratosphere in the summer. In winter, for lead-times larger than 5 days the stratospheric Z is a better predictor of the daily Z(1000) than Z(1000) itself. Whereas the predictive skill of the stratospheric Z is largest for zero lead-time, the predictive skill of the stratospheric Z-Z(1000) and temperature are largest for lead-times of about ten days, evidencing the finite propagation time of geopotential anomalies from the stratosphere to the surface. The skill of the stratospheric height and temperature in predicting the wintertime monthly-mean field of Z(1000), is

mainly limited to the region north of 60ºN. The stratospheric predictive skill for the monthly-mean fields of the zonal wind at 850 hPa and the near-surface temperature is particularly large around 60ºN. The correlation pattern of the near-surface temperature field and the stratospheric temperature is qualitatively similar to the corresponding pattern for the Arctic Oscillation index, except at middle latitudes over Eurasia and over the subtropical Pacific.

1. Introduction

Recent studies have shown that the stratosphere can be used as a predictor of the troposphere on time scales beyond the deterministic time scale of ~10 days. Baldwin *et al*. (2003) applied a statistical model in which the Northern Annular Mode (NAM) at levels between 1000 and 10 hPa was used to predict the monthly-mean Arctic Oscillation (AO). The NAM was defined at each level as the leading empirical orthogonal function (EOF) of slowly varying hemispheric geopotential at that level, and the AO was defined as the NAM at 1000 hPa. Their results show that the predictability of the AO is greatest in winter, and that the stratospheric NAM is a better predictor of the AO than the AO itself. Charlton *et al*. (2003) demonstrated that using the stratospheric NAM as a predictor of the AO results in a gain of skill of ~5% over a troposphere-only predictor. Christiansen (2004) computed statistical forecasts, using as predictor the zonal-mean zonal wind at 60ºN at different altitudes in the troposphere and the stratosphere, and as predictands the zonal-mean zonal wind near the surface and the near-surface temperature in northern Europe. His results show that the inclusion of stratospheric information increases the skill of the daily forecast on lead-times larger than 5 days. The sensitivity of the troposphere to the stratosphere was further illustrated by Charlton *et al*. (2004), who showed that forecasts of the troposphere, computed with a high resolution numerical weather prediction model, significantly depend on the initial state of the stratosphere.

The geopotential height in the stratosphere, from which predictors are computed by Baldwin *et al*. (2003) (hereafter denoted as B2003) and Charlton *et al*. (2003), not

only depends on the state of the stratosphere but also on the state of the troposphere. In particular, it depends, as expressed by Eq. (1), on the sea-level pressure, the temperature in the troposphere and the temperature in the stratosphere:

$$Z(p) = Z(1000) + \frac{R}{g}\int_{p}^{1000} \frac{T}{p'} dp', \qquad (1)$$

where $Z(p)$ is the geopotential height at the (stratospheric) pressure level p, $Z(p)$ and p are in units of meters and hPa, respectively, and the other symbols have their usual meteorological meaning. The $Z(1000)$ is related to sea-level pressure (*SLP*) by the approximate relation SLP=1000+0.121 $Z(1000)$ (Peixoto and Oort, 1992, Section 7.1.2). Thus, the predictive skill of the stratospheric height not only depends on the state of the stratosphere itself, i.e. on stratospheric temperature, but in addition on the state of the troposphere, i.e. on tropospheric temperature and sea-level pressure.

New in the present study is that the predictive skill of the stratosphere itself will be studied, i.e. using the stratospheric temperature rather than the stratospheric geopotential or NAM as predictor. In addition, the predictive skill of *Z(p)* will be studied, as well as that of *Z(p)-Z(1000).* In the latter predictor the contribution to the predictive skill of *Z*(p) by sea-level pressure is virtually eliminated. The predictors will be computed as averages of these quantities over the polar cap north of 65ºN. One advantage of using these predictors is that they can be computed relatively easy from atmospheric circulation data. A second advantage is that for the polar cap-mean stratospheric temperature the actual values are available on the Web, via http://www.cpc.ncep.noaa.gov/products/stratosphere/temperature/, facilitating the construction of actual extended-range forecasts. As predictands the polar cap-mean

Z(1000), and geographical fields of Z(1000), the zonal wind at 850 hPa, and the 2-meter temperature will be used. Geographical fields as predictand have not been used before in studies on stratospheric predictive skill. The predictive skill for the polar cap-mean Z(1000) will be investigated for different lead-times and different averaging periods of the predictors and the predictands.

2. Data and method

The predictors and predictands are computed each day at 12 UTC of the period 1958-2001, using analyses of the European Centre for Medium-Range Weather Forecasts (ECMWF) 40-year reanalysis (ERA-40) dataset (Simmons and Gibson, 2000). They are computed at the 23 pressure levels for which these data are available, i.e. 1, 2, 3, 5, 7, 10, 20, 30, 50, 70,100, 150, 200, 250, 300, 400, 500, 600, 700, 775, 850, 925, and 1000 hPa. The horizontal resolution of the data is 2.5º latitude by 2.5º longitude. The predictors are, except for one result presented at the end of Section 3d, instantaneous values valid at time t_1, whereas the predictands are averages over the period from t_1+t_0 to $t_1+t_0+\tau$, where t_0 is the lead-time and τ is the averaging period.

The predictive skill will be expressed in terms of the percent variance, which is the fraction of the variance of the predictand that is accounted for by the predictor in a linear least-square regression, multiplied by 100%. This fraction is equal to the square of the correlation coefficient. The predictors and predictands are time series of 44 elements (N=44), corresponding to a specific calendar-day of the years 1958-2001. Using a two-sided Student-t test with the statistic $t=r((N-2)/(1-r^2))^{½}$ to test the significance of a nonzero correlation coefficient r, it follows that r is significantly

nonzero at a 95%-level if its magnitude is larger than 0.30, corresponding to a percent variance larger than 9%.

3. Results

a. The annual cycle of the polar cap-mean geopotential height

We will first consider the time-height distribution of the geopotential height, averaged over the polar cap north of 65ºN. This quantity is one of the predictors used in this study. To highlight interannual variations, anomalies are considered, which are the deviations from the long-term (1958-2001) mean annual cycle. To obtain comparable magnitudes at different pressure levels, the anomalies at each level are divided by the standard deviation of the total 44-year time series of the anomalies at that level. This scaled geopotential height anomaly will hereafter be denoted as Z^*. Fig. 1 shows the time-height distribution of Z^*. Note that prior to scaling the geopotential has been low-pass filtered by computing its 91-day average, and for conciseness only the period 1983-1997 is shown. This distribution is very similar, both qualitatively and quantitatively, to the corresponding distribution of the AO-signature in the geopotential height as shown by Baldwin and Dunkerton (1999, their Fig. 6) for levels up to 10 hPa. Thus, the downward propagation that occurs in the AO-signature time series is displayed similarly by the more easily computable polar cap-mean geopotential height.

The long-term mean annual cycle of $(Z^*)^2$ as a function of height is shown in Fig. 2a for unfiltered data, and in Fig. 2b for low-pass filtered data. In Fig. 2a the daily

values of the long-term mean of $(Z^*)^2$ have been averaged using Gaussian weighting with a full width at half maximum of 60 days. As a result of the scaling, the annual average of the long-term mean of $(Z^*)^2$ is at all levels equal to one. The largest values of the unfiltered $(Z^*)^2$ occur in January and February throughout the entire stratosphere. The largest low-pass filtered values occur in December and January in the upper stratosphere, and about one month later in the lower stratosphere. The low-pass filtered distribution shows a second maximum during winter near the surface about one month later than the maximum in the stratosphere.

b. Predictive skill of Z(p), Z(p)-Z(1000), and T(p)

We will now consider the skill of the polar cap-mean geopotential height at different levels in the troposphere and the stratosphere in predicting the polar cap-mean geopotential height at 1000 hPa. This predictand can be considered as a proxy of the AO-index. Monthly values for December, January and February 1958-2001 of the two quantities have a correlation of –0.94. The applied AO-values are those obtained by Thompson and Wallace (2000). As the AO-index has shown to be significantly related to weather in many regions (see, e.g., Thompson and Wallace 1998, 2000 and 2001; Gong *et al*., 2001; Kryjov, 2002; Bamzai, 2003), the large correlation implies that the same is true for the polar cap-mean $Z(1000)$. The predictor is the daily $Z(p)$ at 12 UTC at the available 23 pressure levels from 1000 hPa to 1 hPa, and the predictand $Z(1000)$ is averaged over a period τ of one month (31 days), with a lead-time t_0 of 10 days. These values of τ and t_0 were also used by B2003. The percent variance of $Z(1000)$ accounted for by $Z(p)$, as a function of pressure altitude and time of the year of the predictor, is shown in Fig. 3a. The daily values of the percent variance have

been averaged using the same Gaussian weighting as in Fig. 2a, similar to the corresponding result of B2003 (their Fig. 2). The maximum values of the percent variance, about 22%, occur at 50 hPa at the end of December. Thus, the best predictable 31-day mean of $Z(1000)$ is about the January-mean. Percent variances larger than 10%, which are significantly non-zero at a more than 95% level, exist from November through March. The maximum value in Fig. 3a is only slightly smaller than the maximum of about 24% that was found by B2003. In B2003 the maximum occurs at a lower level, about 150 hPa, and later in the winter, in early February. In B2003 the maximum at the end of December occurs near 100 hPa, and has nearly the same value as in the present study. At 50 hPa the present values are slightly larger than those in B2003. Like in B2003, a secondary maximum occurs in winter near the surface. Its value, about 11%, is, however, much smaller than the 19% found by B2003 (see their Fig. 2b).

The stratospheric geopotential height is, as expressed by Eq. (1), determined both by sea-level pressure, or $Z(1000)$, and by the vertical temperature distribution, or $Z(p)$-$Z(1000)$. When using $Z(p)$-$Z(1000)$ as a predictor instead of $Z(p)$, the effect of sea-level pressure on the predictive skill is eliminated. Fig. 3b shows the analogue of Fig. 3a, but with $Z(p)$-$Z(1000)$ as predictor instead of $Z(p)$. The differences between Figs. 3a and 3b are very small, except in the troposphere, where the predictive skill of $Z(p)$ is relatively large, but that of $Z(p)$-$Z(1000)$ is very small. Thus, the predictive skill of $Z(p)$ in the troposphere is mainly determined by $Z(1000)$, whereas in the stratosphere it is mainly determined by $Z(p)$-$Z(1000)$, equivalent to an integral over the vertical temperature distribution. Although the stratospheric $Z(p)$-$Z(1000)$ is determined by the temperature in both the troposphere and the stratosphere, the small tropospheric

and large stratospheric values in Fig. 3b suggest that the predictive skill of the stratospheric $Z(p)$-$Z(1000)$, and of the stratospheric $Z(p)$, is determined mainly by the predictive skill of the stratospheric temperature. To investigate this, Fig. 3c shows the analogue of Figs. 3a,b, but with the polar cap-mean temperature as predictor. Indeed in the stratosphere the predictive skill of the temperature is much larger than in the troposphere. The largest percent variance occurs, rather uniformly, between about 250 hPa and 50 hPa, from the middle of December to the middle of January. Here its value is about 18%, which is slightly smaller than the largest values for the predictors $Z(p)$ (Fig. 3a, 22%) and $Z(p)$-$Z(1000)$ (Fig. 3b, 20%). Although the stratospheric geopotential height is a slightly better predictor of $Z(1000)$ than the stratospheric temperature, it is concluded that in the winter the latter quantity is still a useful predictor. In the winter the predictive skill of the temperature in the upper stratosphere is small compared to that in the lower stratosphere. Thus, the large predictive skill of $Z(p)$ in the wintertime upper stratosphere (Fig. 3a) is mainly due to the predictive skill of the temperature in the lower stratosphere. Fig. 3c shows that during summer the temperature has a statistically significant predictive skill in the upper stratosphere. This predictive skill could be a manifestation of the influence of solar variability on the climate of the troposphere (Haigh, 2003). Although the stratospheric height and temperature are predictors of the weather at the extended range, it should be noted that the physical reasons why the stratosphere affects surface weather may depend (in part) on other quantities, such as the wind field.

To test the predictability of $Z(1000)$, we performed a cross-validated forecast, in which artificial skill is avoided. We removed one year at a time, and predicted for the removed year the value of $Z(1000)$, using the linear least-squares regression

coefficients that were computed from the remaining 43 years. This was done separately for each calendar day and each level of the predictor Z(p). The resulting cross-validated skill as a function of pressure altitude and time of the year of the predictor Z(p) is shown in Fig. 3d. In the wintertime lower stratosphere the maximum predictive skill drops from 22% in Fig. 3a to 15% in Fig. 3d. Thus, of the predictive skill in Fig. 3a about one third is artificial skill. In the troposphere, Fig. 3d shows no significant predictive skill. Thus, when Z(1000) is actually predicted with this scheme, Z(p) is a useful predictor only at lower stratospheric levels.

Actual extended-range forecasts based on the actual stratospheric temperature can be made as follows. The linear least-squares regression line relating the actual stratospheric temperature, T_a, and the predicted value of Z(1000), $Z_p(1000)$, is given by

$$\frac{Z_p(1000) - [Z(1000)]}{\sigma(Z(1000))} = r\frac{T_a - [T]}{\sigma(T)}, \qquad (2)$$

where $[x]$ and $\sigma(x)$ are, respectively, the long-term mean and the standard deviation (or interannual variability) of x, and r is the correlation coefficient of Z(1000) and T. The standard deviation of Z_p(1000) is equal to $\sigma(Z(1000))(1\text{-}r^2)^{1/2}$. With Eq. (2) the deviation of Z_p(1000) from its long-term mean value, in units of $\sigma(Z(1000))$, can be predicted from T_a, if the values of $[T]$, $\sigma(T)$, and r are known. The value of T_a can be obtained, for example, from the website mentioned in Section 1. This will be illustrated for T and Z(1000) as used in Fig. 3c, where T is taken at the 70 hPa level. The annual cycles of $[T]$ and $\sigma(T)$, computed from the ERA-40 data of the period 1958-2001, are shown in Fig. 4. The annual cycle of r^2 (*100%) is shown in Fig. 3c.

Here the large values of r^2 in the wintertime lower stratosphere correspond to positive values of r. A value, for example, of T_a = -60 ˚C on 1 January ([T]= -66.3 ˚C, $\sigma(T)$= 4.6 ˚C, and r=(0.19)^{½}) gives (Z_p(1000)–[Z(1000)])/σ(Z(1000))=0.6, i.e. Z_p(1000) is predicted to be 0.6 standard deviations larger than its long-term mean value; here Z_p(1000) is the predicted average over the one-month period starting on 11 January. The values of [Z(1000)] and σ(Z(1000)) are about 100 m and 50 m, respectively, throughout the winter. Thus, Z_p(1000) = 130 m, with a standard deviation of 45 m, corresponding to a sea-level pressure of 1016 hPa, with a standard deviation of 5 hPa.

c. Predictive skill for different lead-times

The differences between the skills of $Z(p)$ and $Z(p)$-Z(1000) in predicting Z(1000) become particularly visible when they are considered as a function of altitude and lead-time, as shown in Figs. 5a,b. The percent variance has been averaged over the months December, January and February (DJF), when, as shown in Fig. 3a, its values are largest; no Gaussian or other weighting has been applied. Both the predictor and the predictand are instantaneous values at 12 UTC, unlike in Fig. 3, where the predictand is an average over 1 month. As shown in Fig. 5a, for lead-times $t_0 \leq 5$ days, the predictive skill of Z(p) is largest at the surface. From t_0=5 days to t_0=6 days, however, the level of largest skill jumps from the surface to the 150 hPa level. For further increasing t_0 the pressure level of maximum skill gradually further decreases, to 30 hPa for t_0 larger than about one month. Thus, for lead-times larger than 5 days the stratospheric $Z(p)$ is a better predictor of Z(1000) than the tropospheric $Z(p)$. This agrees with the results of Christiansen (2004), who used the zonal mean zonal wind at 60°N as predictor and predictand. Although Fig. 5 qualitatively agrees with

the corresponding result by Christiansen (2004, his Fig. 5), his predictive skill values are generally larger than those in the present study. An explanation for this might be the difference in the used predictor and predictand. Between 1000 hPa and 70 hPa the skill is largest at t_0=0. This is what 'normally' is expected for a predictor, as normally the near future is better predicted than the distant future. At higher levels, however, the value of t_0 with largest skill increases from 1 day at 50 hPa, 3 days at 20 hPa, to about 20 days above 10 hPa. These results indicate that the skill of $Z(p)$ in predicting $Z(1000)$ is governed by three aspects: strength, memory and delay. The strength of the tropospheric skill is large, but due to the short tropospheric memory it persists only for small lead-times. The strength of the stratospheric skill is small, but due to the longer stratospheric memory it persists for longer lead-times. The delay that exists at levels above 70 hPa evidences the non-zero time required for downward propagation of signals from the stratosphere to the surface.

The corresponding pattern for the predictor $Z(p)$-$Z(1000)$ (Fig. 5b) is very different from that for $Z(p)$ (Fig. 5a). Unlike for $Z(p)$, for small lead-times the predictive skill of $Z(p)$-$Z(1000)$ is small at all levels. Thus, the relatively large skill of $Z(p)$ for small lead-times is, both in the troposphere and in the stratosphere, due to the skill of $Z(1000)$. The skill of $Z(p)$-$Z(1000)$ is largest around 100 hPa for lead-times of about one to two weeks. The skill of $Z(p)$-$Z(1000)$ in predicting $Z(1000)$ is determined by two aspects: memory and delay. Due to the finite memory of the stratosphere, the predictive skill will, like that of a 'normal' predictor, decrease with increasing lead-time. On the other hand, the non-zero downward propagation time of signals from the stratosphere to the 1000 hPa level causes a delay in predictive skill. The net effect of these two aspects is that with increasing lead-time the skill increases for small lead-

times, and decreases for large lead-times. The corresponding pattern for the predictor $T(p)$ is very similar to that for $Z(p)$-$Z(1000)$ (not shown).

d. Predictive skill for different averaging periods of the predictand and the predictor

We will now consider the DJF-averaged skill of $Z(p)$ in predicting $Z(1000)$ as a function of altitude and averaging period τ, using lead-times t_0 of 0 days (Fig. 6a) and 10 days (Fig. 6b). If t_0=0 days and τ less than about two weeks, then the best predictor of $Z(1000)$ is $Z(1000)$ itself. For larger τ, however, the best predictor is at stratospheric levels. For example, the best predictor for the monthly-mean $Z(1000)$ (τ=31 days) is $Z(100)$. The level of largest predictive skill slightly increases with increasing value of τ, up to 50 hPa for τ more than two months. Whereas for tropospheric predictors the predictive skill is largest for τ=1 day (i.e.: no averaging), for stratospheric predictors the largest skill occurs for a longer averaging period. For example, the largest predictive skill of $Z(100)$ occurs for a value of τ of about three weeks. Thus, although the skill of $Z(100)$ of predicting individual days (τ=1 day) decreases with increasing lead-time (see Fig. 5a), for predicting time-averages the skill increases with increasing averaging period, as long as this period is less than about three weeks. This effect is even stronger for predictions with a lead-time of 10 days (Fig. 6b). Note that the skill for τ=1 in Figs. 6a and 6b is equal to the skill for, respectively, t_0=0 days and t_0=10 days in Fig. 5a. The skill in Fig. 6b is largest between 70-100 hPa, for values of τ of about two weeks. For averaging periods of more than three weeks, $Z(50)$ is the best predictor. The maximum in the stratospheric predictive skill in Fig. 6a and, particularly, in Fig. 6b can be interpreted as the result of two competing effects. Firstly, the predictive skill for an average over a period τ

increases with increasing τ. Secondly, the average skill for the individual days decreases with increasing τ. The first effect tends to increase the skill with increasing τ and dominates for small τ, whereas the second tends to decrease the skill and dominates for large τ. Consequently, there is an averaging period τ where the skill is at a maximum.

As the predictive skill is largest during winter (see Fig. 3), in Figs. 5 and 6 the attention was restricted to DJF-averages. However, also within the winter there are considerable differences in predictive skill. This is illustrated in Fig. 7a, which shows the skill of $Z(50)$ in predicting Z(1000) as a function of averaging period τ and, like in Fig. 3, time of the year of the predictor, using a lead-time of 10 days. The results have been filtered in the same way as those in Fig. 3. Note that the skill for τ=31 days in Fig. 7a is the same as that for 50 hPa in Fig. 3a. As expected, the skill is largest during winter, but is different for different parts of the winter. The tilted pattern shows that the value of τ for which the skill is largest decreases during the course of the winter. If, however, the time at the horizontal axis is defined as the centre of the period over which the predictand is averaged (Fig. 7b), rather than as the time of the predictor (Fig. 7a), then the tilting almost disappears and the largest predictive skill occurs in the second half of January, for a large range of τ. Thus, the predictive skill depends more strongly on the centre of the period to which the predictand applies than on the time of the predictor. This may be interpreted as follows. The predictive skill of a stratospheric predictor is expected to increase with increasing stratospheric persistence and with increasing strength of the coupling between the stratosphere and the surface. The strength of the coupling can presumably be approximated by the strength at the centre of the averaging period. The absence of tilting in Fig. 7b,

therefore, suggests that the seasonal variations in predictive skill are mainly due to seasonal variations in the strength of the coupling, and not to variations in persistence. The latter point is confirmed by the small variation of the $1/e$ (~0.37) autocorrelation time-scale of $Z(50)$ during December, January and February. For these months we computed a mean value of 29.6 days, with a daily standard deviation of only 3.7 days.

In the results presented above the predictors are instantaneous values at time t_1. The question arises whether the predictive skill would increase if, in addition, the predictor would include information from prior to t_1. Although intuitively it might be assumed that the future is better predicted by the present than by the past, Figs. 5a,b show that this is not always true for stratospheric predictors, and Fig. 6b shows that stratospheric predictors can better predict time-averaged than instantaneous predictands. The DJF-averaged skill of $Z(p)$ in predicting $Z(1000)$ as a function of altitude and averaging period τ of the predictor is shown in Fig. 8. Here the predictor is averaged over the period $[t_1 - \tau, t_1]$. The lead-time is 10 days, and the predictand is averaged over a period of 31 days (i.e. the predictand is averaged over the period $[t_1 + 10, t_1 + 40]$). For predictors in the upper stratosphere the predictive skill indeed slightly increases with increasing averaging period of the predictor, but in the lower stratosphere, where the predictive skill is largest, the skill decreases with increasing averaging period. Thus, the best predictor of $Z(1000)$ is the instantaneous geopotential height in the lower stratosphere.

e. Predictive skill for geographical fields as predictand

In the results presented above, the predictand is the average of $Z(1000)$ over the entire area north of 65ºN. In the present subsection the predictand will instead be the geographical field of $Z(1000)$ in the Northern Hemisphere. The predictor is the daily $Z(50)$ averaged over the area north of 65ºN, which was shown above to give the largest predictive skill of the area-mean of $Z(1000)$ (see Fig. 3a). In addition, the skill of the area-mean $Z(50)$ in predicting the geographical fields of the zonal wind at 850 hPa ($U(850)$) and the near-surface (2 meter level) temperature (T_{2m}) will be considered. Anomaly monthly-means of these fields for December, January and February 1958-2001 have been correlated with the anomaly daily area-mean $Z(50)$, using a lead-time of 10 days. For example, the December-mean has been correlated with $Z(50)$ on 21 November. The anomalies are deviations from the long-term mean (1958-2001) annual cycle. For a time series of 3*44 elements, the correlation significantly deviates from zero at a 95% level if its magnitude is larger than 0.2.

The field of the correlation between $Z(50)$ and the field of $Z(1000)$ (Fig. 9a) is dominated by a dipole pattern over the Atlantic sector, with positive values larger than 0.3 in the Arctic, and negative values less than -0.3 around 45ºN. If the $Z(1000)$ averaged over the area north of 65ºN is used as predictor of the field of $Z(1000)$ (Fig. 9b), then the positive correlations in the Arctic become much smaller, whereas the negative correlations at middle latitudes weaken only slightly. Thus, only in the polar region the stratospheric polar cap-mean geopotential is a better predictor of $Z(1000)$ than the polar cap-mean of $Z(1000)$ itself. The correlation map between $Z(50)$ and $U(850)$ (Fig. 9c) is physically consistent with the correlation between $Z(50)$ and the meridional pressure gradient that can be inferred from Fig. 9a. A positive $Z(50)$ anomaly corresponds to a weaker than average pressure gradient around 60ºN, which

in turn corresponds to a negative $U(850)$ anomaly. Similarly, a positive $Z(50)$ anomaly corresponds to a stronger than average pressure gradient south of the middle latitude minimum in Fig. 9a, which in turn corresponds to a positive $U(850)$ anomaly. The correlation map between $Z(50)$ and T_{2m} (Fig. 9d) is consistent with that of $Z(50)$ and $U(850)$. If the $Z(50)$ anomaly is positive, then the negative $U(850)$ anomaly around 60ºN induces a negative T_{2m} anomaly over Siberia, less influenced by the relatively warm westward oceans, and a positive T_{2m} anomaly between Canada and Iceland, less influenced by the cold North American winter continent. Similarly, the positive $U(850)$ anomaly at middle latitudes induces a positive T_{2m} anomaly over the Mediterranean. In these regions the near-surface temperature anomalies are much better predicted by the polar cap-mean $Z(50)$ than by the polar cap-mean $Z(1000)$ (Fig. 9e). The negative anomaly east of Florida, on the other hand, is better predicted by the polar cap-mean of $Z(1000)$ than by the polar cap-mean of $Z(50)$. For geopotential height predictors at other levels within the range of 30-100 hPa, or for temperature predictors within this range, the correlation fields are similar to that for the Z(50) predictor, but with slightly smaller magnitudes. As an example, Fig. 9f shows the correlation between the field of T_{2m} and the polar cap-mean temperature at 70 hPa ($T(70)$). Although for this predictor the magnitude of the correlations around 60ºN is slightly smaller than those for the Z(50) predictor (Fig. 9d), they are larger than those for the $Z(1000)$ predictor (Fig. 9e).

Recent studies have shown a significant correlation between the temperature of the polar lower stratosphere and the AO-index (e.g. Thompson and Wallace, 2000; Hartmann *et al.,* 2000). This raises the question about the similarity of the correlation patterns of $T(70)$ and of the AO-index with the surface temperature field. Fig. 10a

shows the correlation pattern of the AO-index with the field of T_{2m}. This result has been computed using monthly AO-indices (Thompson and Wallace, 2000) and monthly temperature anomalies for December, January and February 1958-2001. Although Fig. 10a resembles in several aspects the correlation pattern of $T(70)$ with the field of T_{2m} (Fig. 9f), there are important differences. To facilitate the comparison of Fig. 10a with Fig. 9f, the AO-index has been multiplied by minus one. Both correlation patterns show positive values over Northern Africa and between Canada and Iceland, and negative values over Siberia and east of Florida. One obvious difference concerns the magnitude of the correlations, which is much larger in the AO-pattern. Two other important differences concern the negative correlation patterns over Eurasia. Firstly, the AO-pattern has a strong minimum both over Scandinavia and over Siberia, whereas the $T(70)$-pattern only has a minimum over Siberia. Secondly, in the AO-pattern the minimum over Siberia is around (120°E, 45°N), whereas in the $T(70)$-pattern the minimum has shifted northward to about (120°E, 60°N). The correlation pattern of the monthly $T(70)$ and the monthly T_{2m} anomalies for DJF is shown in Fig. 10b. The similarity with Fig. 9f is large, indicating that the lag-time between $T(70)$ and T_{2m} (10 days in Fig. 9f, no lag in Fig. 10b) and the type of averaging of $T(70)$ (daily values in Fig. 9f, monthly means in Fig. 10b) has only a weak effect on the correlation with the field of T_{2m}. Figs. 10a,b show that the correlations of the near-surface temperature field with the polar cap-mean stratospheric temperature and with the AO-index are qualitatively similar. However, there are several important differences. For example, at the middle latitudes of Eurasia, including a large part of Western Europe, the correlation with the AO-index is significantly positive (i.e., negative values in Fig. 10a), but the correlation with the stratospheric temperature is close to zero. Also large differences

occur over the subtropical Pacific, where Fig. 10b shows a dipole whereas Fig. 10a does not. Thus, although the polar cap-mean lower stratospheric temperature and the AO-index are significantly correlated, there exist important differences between the correlation patterns of the two indices with the near-surface temperature field.

4. Summary

This study was motivated by previous studies showing that during winter the stratospheric NAM, derived from the geopotential height, has substantial skill in predicting the time-averaged lower troposphere at the extended range. Since the stratospheric geopotential height depends on sea-level pressure, tropospheric temperature, and stratospheric temperature, we questioned whether the stratospheric predictive skill is mainly due to the stratosphere itself, i.e. to the stratospheric temperature, or whether there are substantial contributions from the troposphere, particularly from sea-level pressure. In addition, we investigated whether instead of the NAM also the more easily computable polar-cap mean geopotential and temperature can be used as predictors. An additional advantage of the latter quantity is, that its actual stratospheric values are directly available on the Web. As predictands we used the polar-cap mean geopotential height at 1000 hPa ($Z(1000)$), and geographical fields of several near-surface quantities. The predictive skill has been determined for different lead-times between predictor and predictand, and different averaging periods of the predictor and the predictand.

The skill of the stratospheric polar-cap mean geopotential in predicting the polar cap- and monthly-mean $Z(1000)$ is slightly less than that of the stratospheric NAM in

predicting the monthly-mean AO as computed in B2003 (the maximum percent variances are, respectively, 22% and 24%). When the contribution of sea-level pressure to the stratospheric predictive skill is eliminated (Fig. 3b), the maximum reduces to 21%. When the polar-cap mean stratospheric temperature is used as predictor (Fig. 3c), the maximum reduces to 18%. This is more than the predictive skill of $Z(1000)$ (11%, Fig. 3a), but just below the skill of the AO in predicting the monthly-mean AO (19%, B2003). When artificial skill is excluded (Fig. 3d), the maximum reduces to 15%. There is also a significant predictive skill of the temperature in the upper stratosphere in summer, which possibly points to a link between solar variations and surface weather. Given the relatively easy availability of the polar-cap mean predictors, it is concluded that these are useful extended-range predictors. An example of computing the value of the predictand from an (actual) value of the predictor is given in Section 3b. The largest predictive skill of the temperature occurs rather uniformly in the layer between 250 hPa and 50 hPa (Fig. 3c). The optimum single level for forecasting the AO as computed by B2003, 150 hPa, is at the middle of this layer. The largest predictive skill of the geopotential is at the top of this layer (Fig. 3a), as is also suggested by Eq. (1).

Predictive skill results for different lead-times and different averaging periods can be interpreted in terms of strength, memory, and delay. The strength of the tropospheric geopotential as predictor is large, but due to the short tropospheric memory it persists only for a short time (Fig. 5a). The strength of stratospheric predictors is small, but due to the long stratospheric memory the predictive skill persists for a long time. The tropospheric predictive skill is almost entirely due to the predictive skill of sea-level pressure (Figs. 5a,b). Because of the finite downward propagation speed of

geopotential anomalies from the stratosphere to the surface, the response of the surface to the stratosphere is delayed. As a result, for predictors in the upper stratosphere the skill maximizes at lead-times larger than zero (Fig. 5a). If the predictive skill of sea-level pressure is excluded, then the skill maximizes in the lower stratosphere at a lead-time of about ten days (Fig. 5b). This suggests that the time of downward propagation from the lower stratosphere to the surface is about ten days. With increasing averaging period, the predictive skill for a time-averaged predictand tends to increase due to the decrease of 'noise', but tends to decrease due to the decreased predictive skill for the individual days in the period. As a result, there exists an averaging period with a maximum skill, which for a lead-time of 10 days is about two weeks (Fig. 6b). Any averaging of the predictor, for this lead-time, decreases the predictive skill (Fig. 8).

The field correlation results show that the stratospheric height and temperature are a better predictor of the monthly-mean $Z(1000)$ than $Z(1000)$ itself in the entire region north of 60ºN. Additional stratospheric skill in predicting the monthly-mean $U(850)$, however, is limited to the edge of this region. This suggests that the monthly-mean response of $Z(1000)$ to the state of the stratosphere is rather uniform in this region, leading to additional stratospheric skill in predicting the monthly-mean meridional lower tropospheric pressure gradient, and the related $U(850)$, only near the edge of this region. The additional stratospheric skill in predicting the monthly-mean near-surface temperature is limited to those regions around 60ºN where this temperature strongly depends on the zonal wind, particularly Siberia and the western Atlantic. The near-surface temperature field correlates in a similar way with the polar cap-mean

stratospheric temperature as with the AO-index, except at middle latitudes over Eurasia and over the subtropical Pacific.

Although the focus of this study is on extended-range weather predictability, some of the results may also be relevant for the wider subject of stratosphere-troposphere coupling. This coupling plays an important role not only in weather-related phenomena but also in climate change (e.g., Shindell *et al.,* 1999; Gillet *et al*., 2003; Sigmond *et al*., 2004). The dynamical mechanism of the coupling is currently under discussion in the literature (e.g., Polvani and Kushner, 2002; Norton, 2003; Sigmond *et al.* 2003; Charlton *et al*., 2004). Our results (Fig. 3a) show, that the predictive skill of the stratospheric temperature is largest, and uniformly large, between 250 and 50 hPa. Thus the largest stratospheric predictive skill does not arise just from a shallow layer directly above the tropopause, as suggested by Baldwin *et al*. (2003), but from the entire layer between the tropopause and 50 hPa. Above 20 hPa the predictive skill of the stratospheric temperature becomes statistically insignificant. On the other hand, the geopotential, which depends on the vertically integrated temperature (Eq. 1), has statistically significant predictive skill at levels up to almost 1 hPa (Figs. 3a and 6). Thus, although stratosphere-troposphere coupling can be detected from information from the upper stratosphere, the origin of the coupling can be in the lower stratosphere. The stratospheric skill at 100 hPa in predicting surface values at individual days is largest for lead-times of about 10 days (Fig. 5b). This lead-time is expected to be the downward propagation time from the 100 hPa level to the surface. Finally, the results suggest (Fig. 7) that the variations during the winter of the stratospheric predictive skill are mainly due to variations in the strength of the

stratosphere-troposphere coupling, whereas variations in the stratospheric persistence only play a minor role.

Acknowledgements

I would like to thank several colleagues for their suggestions and reading, in particular G.J. van Oldenborgh, A.J. Haklander, P.J.F van Velthoven, and W.T.M. Verkley. Stimulating comments from two anonymous reviewers are gratefully acknowledged.

References

Baldwin, M.P., and Dunkerton, T.J., 1999: Propagation of the Arctic Oscillation from the stratosphere to the troposphere. *J. Geophys. Res.,* **104**, 30,937-30,946.

Baldwin, M.P., Stephenson, D.B., Thompson, D.W.J., Dunkerton, T.J., Charlton, A.J., O'Neill, A., 2003: Stratospheric memory and extended-range weather forecasts. *Science,* **301,** 636-640.

Bamzai, A.S., 2003: Relationship between snow cover variability and Arctic oscillation index on a hierarchy of time scales. *Int. J. Clim*., **23**(2), 131-142.

Charlton, A.J., A. O'Neill, D.B. Stephenson, W.A. Lahoz, and M.P. Baldwin, 2003: Can knowledge of the state of the stratosphere be used to improve statistical forecasts of the troposphere? *Quart. J. Roy. Meteorol. Soc.,* **129**, 3205-3224.

Charlton, A.J., A. O'Neill, W.A. Lahoz, and A.C. Massacand, 2004: Sensitivity of tropospheric forecasts to stratospheric initial conditions. *Quart. J. Roy. Meteorol. Soc.*, **130,** 1771-1792.

Christiansen, B., 2004: Downward propagation and statistical forecast of the near-surface weather. *J. Geophys. Res*., submitted.

Gillett, N.P., M.R. Allen, and K.D. Williams, 2003: Modelling the atmospheric response to doubled CO_2 and depleted stratospheric ozone using a stratosphere-resolving coupled GCM. *Quart. J. Roy. Meteorol. Soc.,* **129**, 947-966.

Gong, D.Y., and C.H. Ho, 2003: Arctic Oscillation signals in the East Asian summer monsoon. *J. Geophys. Res.,* **108(D2),** 4066, doi:10.1029/2002JD002193.

Haigh, J.D., 2003: The effects of solar variability on the earth's climate. *Phil. Trans. Roy. Soc*., **361**, 95-111.

Hartmann, D.L., J.M. Wallace, V. Limpasuvan, D.W.J. Thompson, and J.R. Holton, 2000: Can Ozone Depletion and Greenhouse Warming Interact to Produce Rapid Climate Change? *Proc. Nat. Acad. Sci*., **97**, 1412-1417.

Kryjov, V.N., 2002: The influence of the winter Arctic Oscillation on the northern Russia spring temperature. *Int. J. Climatol*., **7**, 779-785.

Norton, W.A., 2003: Sensitivity of northern hemisphere surface climate to simulation of the stratospheric polar vortex. *Geophys. Res. Lett*., **30**, 1627, doi:10.1029/2003GL016958.

Peixoto J.P., and A.H. Oort, 1992. Physics of Climate. American Institute of Physics, 520 pp.

Polvani, L.M., and P.J. Kushner, 2002: Tropospheric response to stratospheric perturbations in a relatively simple general circulation model. *Geophys. Res. Lett.,* **29,** No. 7, doi:10.1029/2001GL014284.

Shindell, D.T., R.L. Miller, G.A. Schmidt, and L. Pandolfo 1999: Simulation of recent northern winter climate trends by greenhouse gas forcing. *Nature,* **399,** 452-455.

Sigmond M., P. Siegmund, and H. Kelder, 2003: Analysis of the coupling between the stratospheric meridional wind and the surface level zonal wind during 1979-93 NH extratropical winter. *Climate Dynamics*, **21**, 211-219.

Sigmond, M., P. Siegmund, E. Manzini, and H. Kelder, 2004: A simulation of the separate climate effects of middle atmospheric and tropospheric CO_2 doubling. *J. Clim.*, **17**, 2352-2367.

Simmons, A.J., and J.K. Gibson, 2000: The ERA-40 project plan. ERA-40 Project Rep. Series 1, 62 pp.

Thompson, D.W.J., and J.M. Wallace, 1998: The Arctic Oscillation signature in the wintertime geopotential height and temperature fields. *Geophys. Res. Lett*., **25,** 1297-1300.

Thompson, D.W.J., and J.M. Wallace, 2000: Annular Modes in the Extratropical Circulation. Part I: Month-to-Month Variability. *J. Clim,* **13,** 1000-1016.

Thompson, D. W. J., and J. M. Wallace, 2001: Regional Climate Impacts of the Northern Hemisphere Annular Mode. *Science,* **293**, 85-89.

Figure captions

FIG. 1. Time-height distribution of scaled geopotential height anomalies, 1983-1997. The geopotential height is averaged over the polar cap north of 65ºN; the scaled anomaly is the deviation from the 1958-2001 mean annual cycle, divided at each level by the standard deviation of the anomaly time series at that level. The daily data have been low-pass filtered (91-day running average). The contour interval is 0.6; the zero contour is omitted; negative contours are dashed; light shading: larger than 0.6; dark shading: less than -0.6.

FIG. 2. Long-term (1958-2001) mean annual cycle of the square of the scaled geopotential height anomaly, as defined in Fig. 1. a) unfiltered data; b) low pass–filtered data. The contour interval is 0.3; values larger than 2.1 are shaded.
In a) daily values have been averaged using a Gaussian weighting with FWHM of 60 days.

FIG. 3. a) Predictive skill (percent variance) as a function of season and pressure altitude of the predictor $Z(p)$ (in hPa); the predictand is $Z(1000)$; the lead-time is 10 days, and the predictand is averaged over one month. b) and c): as a), but with, respectively, $Z(p)$-$Z(1000)$ and $T(p)$ as predictor. d): as a), but excluding artificial skill. Predictors and predictand are averages over the polar cap north of 65ºN. The Gaussian weighting of daily values is as in Fig. 2a. The contour interval is 2%. Values that are statistically significant at a 95%-level are shaded.

FIG. 4. The annual cycle of the 70-hPa temperature averaged over the area north of 65ºN: 1958-2001 average (solid line, in ºC, left axis) and standard deviation (dashed line, in ºC, right axis).

FIG. 5. Winter (DJF)-averaged predictive skill (percent variance), as a function of lead-time (days) and altitude (hPa) of predictors a) $Z(p)$ and b) $Z(p)$-$Z(1000)$; the predictand is the daily $Z(1000)$. The contour interval is 2%; contour values larger than 50% have been omitted. The shading is as in Fig. 3.

FIG. 6. Winter (DJF)-averaged predictive skill (percent variance), as a function of the averaging period of the predictand $Z(1000)$ (days) and altitude (hPa) of the predictor $Z(p)$; the lead-time is a) 0 days, b) 10 days. The contour interval is 2%; contour values larger than 50% have been omitted. The shading is as in Fig. 3.

FIG. 7. Predictive skill of $Z(50)$ (percent variance), as a function of season and averaging period of the predictand $Z(1000)$; in a) the season corresponds to the time of the predictor, and in b) to the centre of the period over which the predictand is averaged. The lead-time is 10 days. The contour interval is 2%. The weighting of daily values and the shading are as in Fig. 3.

FIG. 8. Winter (DJF)-averaged predictive skill (percent variance), as a function of the averaging period and the pressure altitude of the predictor $Z(p)$. The predictand is the polar cap- and 31 day-averaged $Z(1000)$. The lead-time is 10 days. The contour interval is 2%. The shading is as in Fig. 3.

FIG. 9. a) Winter (DJF)-averaged correlation map between the predictor *Z*(50) and the predictand *Z*(1000). The predictor is the anomaly (deviation from long-term mean) averaged over the area north of 65ºN; the predictand is an anomaly monthly-mean geographical field; the lead-time is 10 days; b): as a), but with *Z*(1000) as predictor; c) and d): as a) but with, respectively, the zonal wind at 850 hPa and the 2- meter temperature as predictand; e) and f): as d) but with, respectively, *Z*(1000) and *T*(70) as predictor. Contour values are 0, ±0.2, ±0.3, ±0.4,…; contours less than or equal to zero are dashed. Values that are statistically significant at a 95%-level are shaded; light shading: larger than 0.2; dark shading: less than -0.2.

FIG. 10. DJF-averaged correlation map between the field of the monthly 2-meter temperature anomalies and a) the monthly AO-index (multiplied by minus one), b) the temperature at 70 hPa averaged over the area north of 65ºN. Contours and shadings as in Fig. 9.

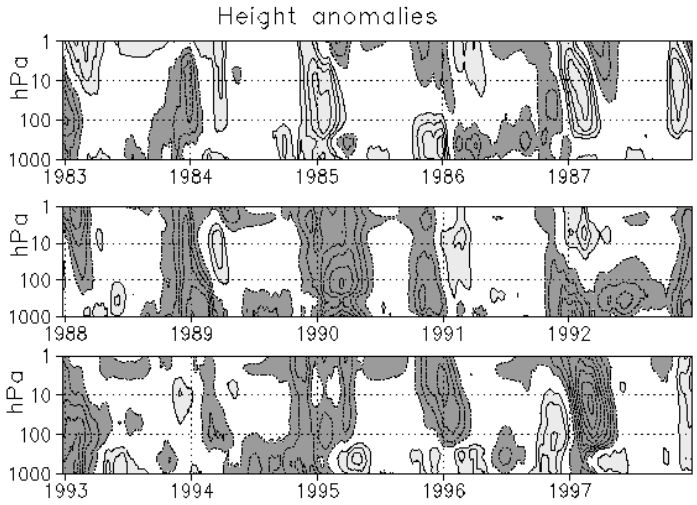

FIG. 1. Time-height distribution of scaled geopotential height anomalies, 1983-1997. The geopotential height is averaged over the polar cap north of 65ºN; the scaled anomaly is the deviation from the 1958-2001 mean annual cycle, divided at each level by the standard deviation of the anomaly time series at that level. The daily data have been low-pass filtered (91-day running average). The contour interval is 0.6; the zero contour is omitted; negative contours are dashed; light shading: larger than 0.6; dark shading: less than -0.6.

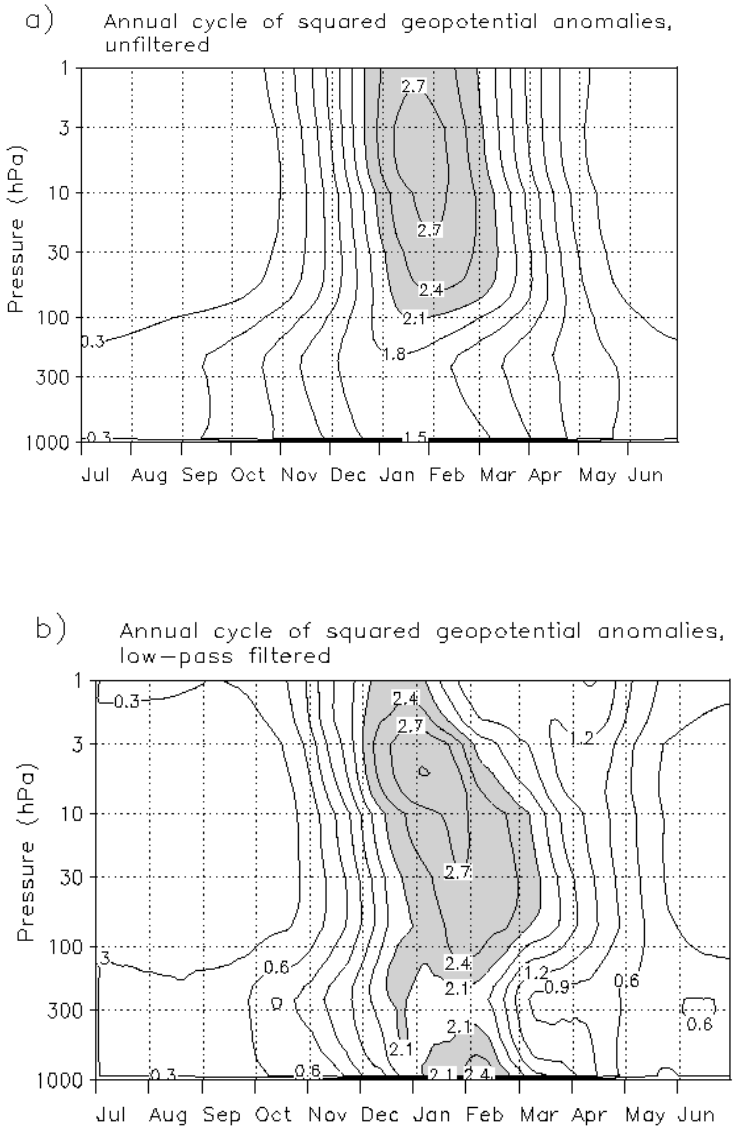

FIG. 2. Long-term (1958-2001) mean annual cycle of the square of the scaled geopotential height anomaly, as defined in Fig. 1. a) unfiltered data; b) low pass–filtered data. The contour interval is 0.3; values larger than 2.1 are shaded.
In a) daily values have been averaged using a Gaussian weighting with FWHM of 60 days.

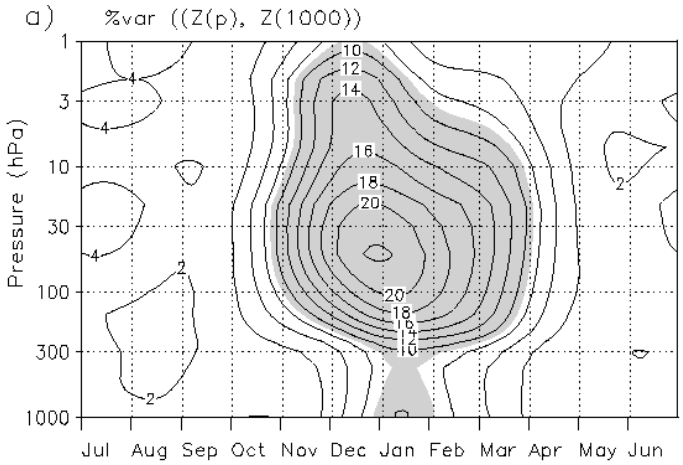
a)
%var ((Z(p), Z(1000))
Pressure (hPa)
1
3
10
30
100
300
1000
Jul Aug Sep Oct Nov Dec Jan Feb Mar Apr May Jun

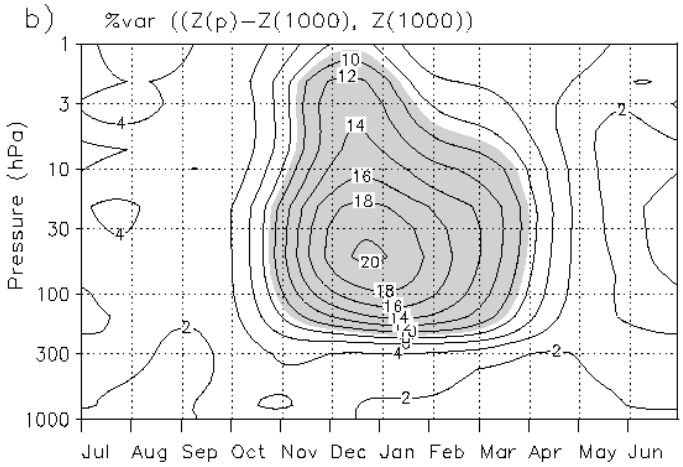
b)
%var ((Z(p)−Z(1000), Z(1000))
Pressure (hPa)
1
3
10
30
100
300
1000
Jul Aug Sep Oct Nov Dec Jan Feb Mar Apr May Jun

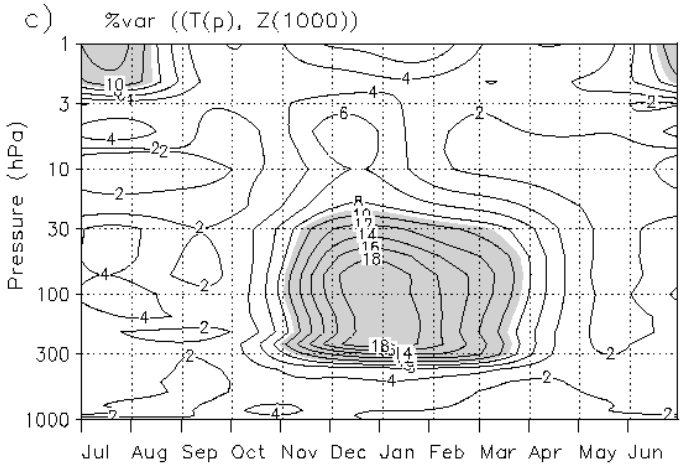
c)
%var ((T(p), Z(1000))
Pressure (hPa)
1
3
10
30
100
300
1000
Jul Aug Sep Oct Nov Dec Jan Feb Mar Apr May Jun

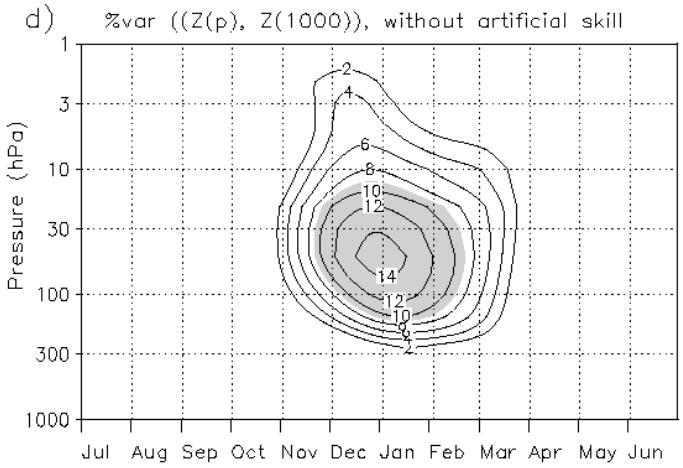

FIG. 3. a) Predictive skill (percent variance) as a function of season and pressure altitude of the predictor $Z(p)$ (in hPa); the predictand is $Z(1000)$; the lead-time is 10 days, and the predictand is averaged over one month. b) and c): as a), but with, respectively, $Z(p)$-$Z(1000)$ and $T(p)$ as predictor. d): as a), but excluding artificial skill. Predictors and predictand are averages over the polar cap north of 65ºN. The Gaussian weighting of daily values is as in Fig. 2a. The contour interval is 2%. Values that are significantly different from zero at a 95%-level are shaded.

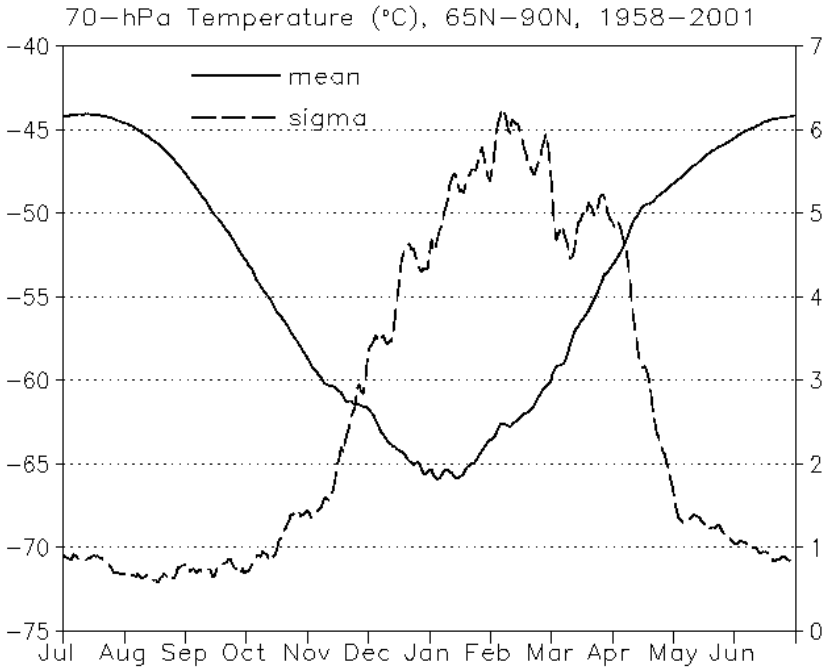

FIG. 4. The annual cycle of the 70-hPa temperature averaged over the area north of 65ºN: 1958-2001 average (solid line, in ºC, left axis) and standard deviation (dashed line, in ºC, right axis).

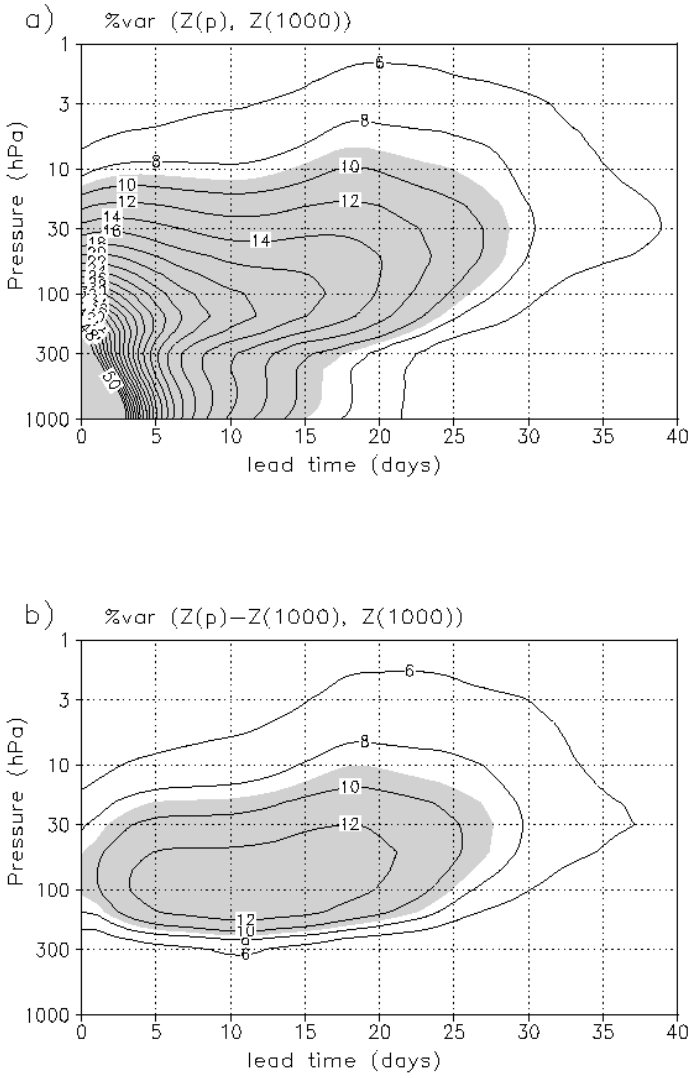

FIG. 5. Winter (DJF)-averaged predictive skill (percent variance), as a function of lead-time (days) and altitude (hPa) of predictors a) $Z(p)$ and b) $Z(p)$-$Z(1000)$; the predictand is the daily $Z(1000)$. The contour interval is 2%; contour values larger than 50% have been omitted. The shading is as in Fig. 3.

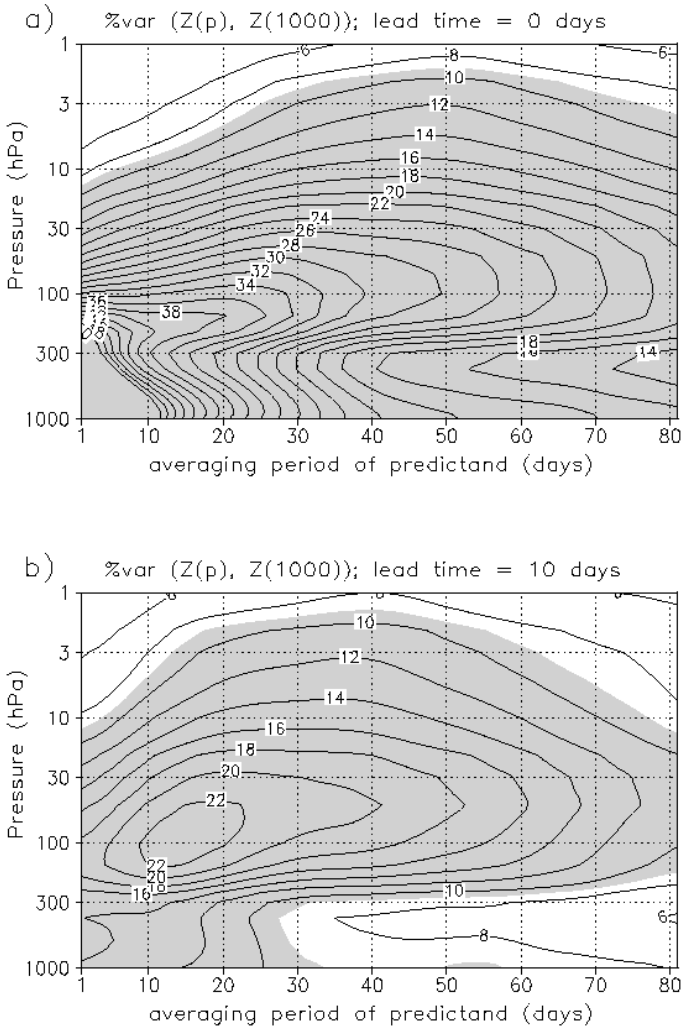

FIG. 6. Winter (DJF)-averaged predictive skill (percent variance), as a function of the averaging period of the predictand $Z(1000)$ (days) and altitude (hPa) of the predictor $Z(p)$; the lead-time is a) 0 days, b) 10 days. The contour interval is 2%; contour values larger than 50% have been omitted. The shading is as in Fig. 3.

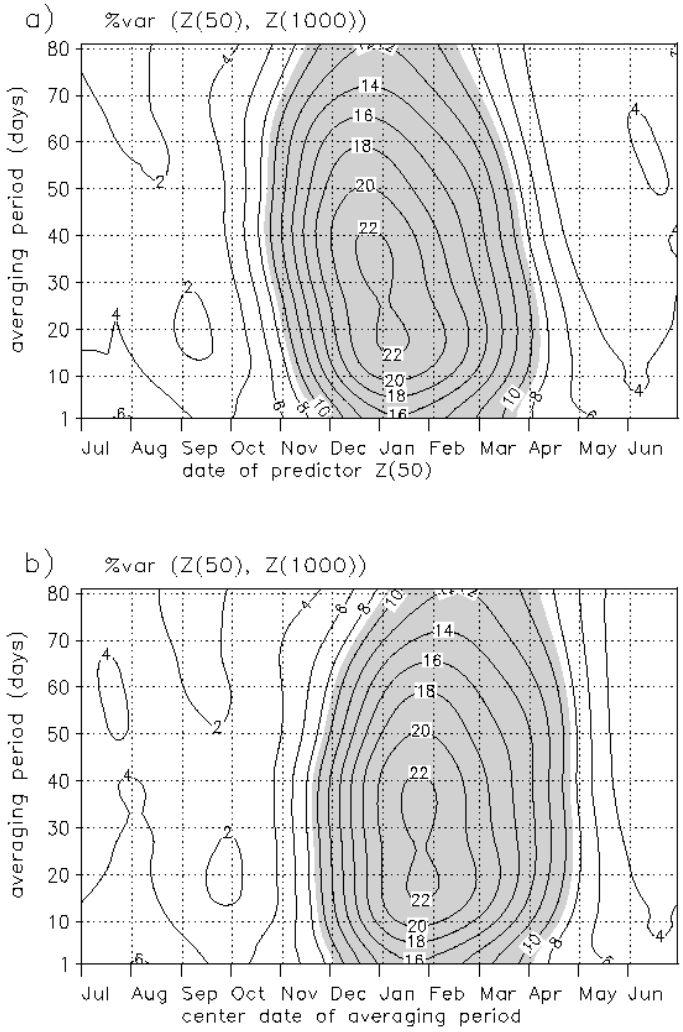

FIG. 7. Predictive skill of *Z*(50) (percent variance), as a function of season and averaging period of the predictand *Z*(1000); in a) the season corresponds to the time of the predictor, and in b) to the centre of the period over which the predictand is averaged. The lead-time is 10 days. The contour interval is 2%. The weighting of daily values and the shading are as in Fig. 3.

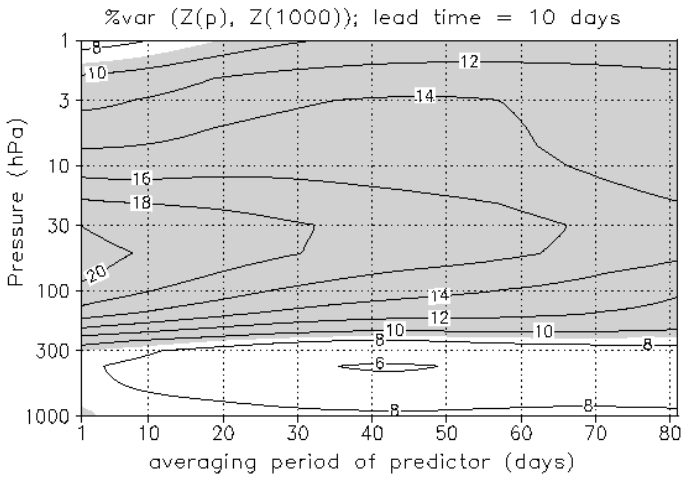

FIG. 8. Winter (DJF)-averaged predictive skill (percent variance), as a function of the averaging period and the pressure altitude of the predictor $Z(p)$. The predictand is the polar cap- and 31 day-averaged $Z(1000)$. The lead-time is 10 days. The contour interval is 2%. The shading is as in Fig. 3.

a)

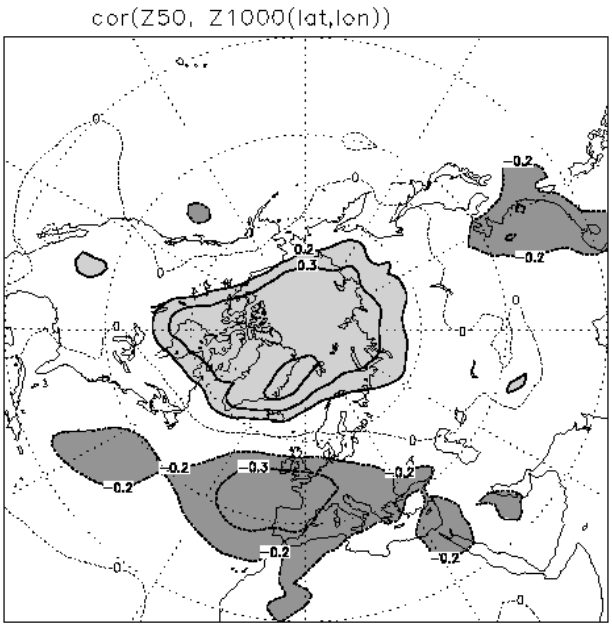
cor(Z50, Z1000(lat,lon))
0
0.2
0.3
-0.2
-0.3

b)

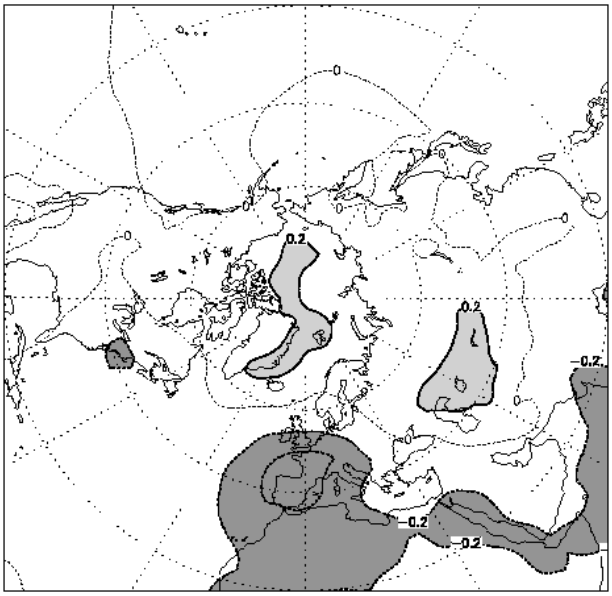
cor(Z1000, Z1000(lat,lon))
0
0.2
-0.2

c)

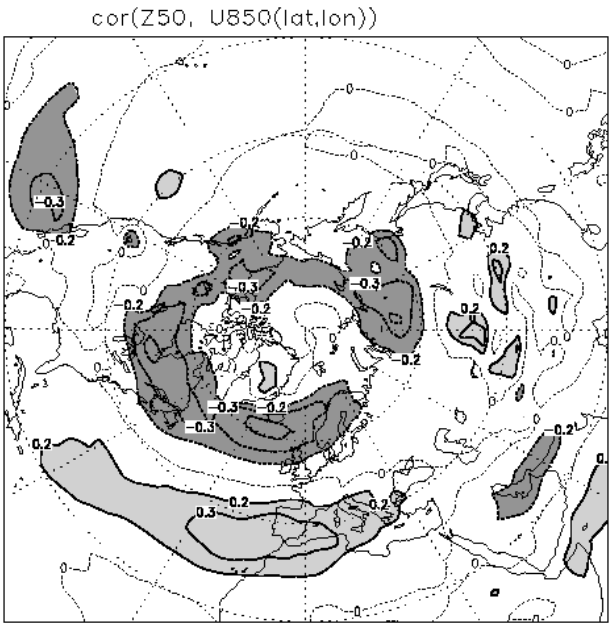

d)

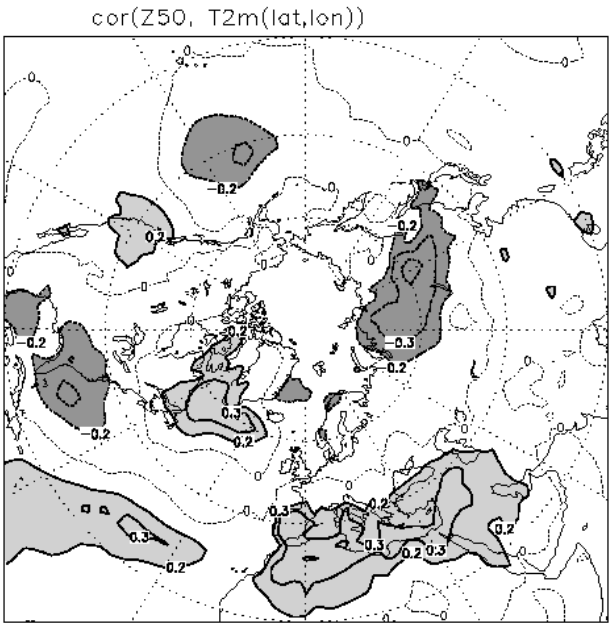

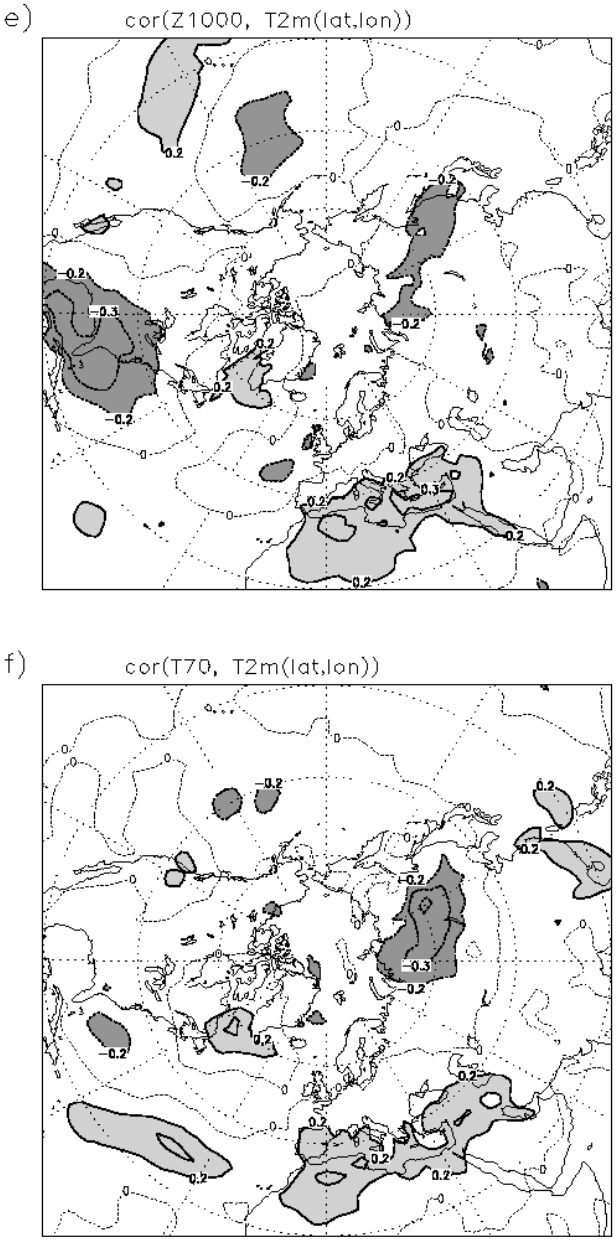

FIG. 9. a) Winter (DJF)-averaged correlation map between the predictor *Z*(50) and the predictand *Z*(1000). The predictor is the anomaly (deviation from long-term mean) averaged over the area north of 65ºN; the predictand is an anomaly monthly-mean geographical field; the lead-time is 10 days; b): as a), but with *Z*(1000) as predictor; c) and d): as a) but with, respectively, the zonal wind at 850 hPa and the 2- meter temperature as predictand; e) and f): as d) but with, respectively, *Z*(1000) and *T*(70) as predictor. Contour values are 0, ±0.2, ±0.3, ±0.4,…; contours less than or equal to zero are dashed. Values that are significantly different from zero at a 95%-level are shaded; light shading: larger than 0.2; dark shading: less than -0.2.

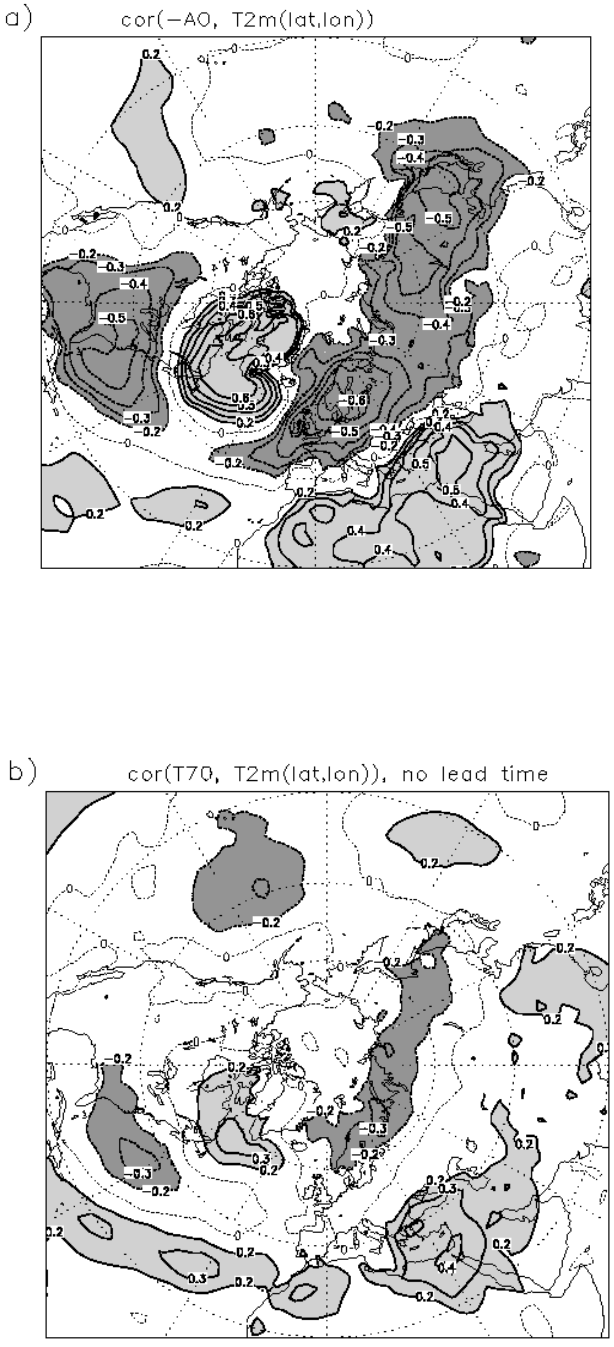

FIG. 10. DJF-averaged correlation map between the field of the monthly 2-meter temperature anomaly and a) the monthly AO-index (multiplied by minus one), b) the temperature at 70 hPa averaged over the area north of 65ºN. Contours and shadings as in Fig. 9.